Exp. Theo. NANOTECHNOLOGY 10 (2026) 1967-1990 https://doi.org/10.56053/10.4.1967

Role of zinc and tin coatings via modified hot-rolling process for corrosion performance of steel rebar in simulated seawater

Sana S. Hameed[1,], Rana A. Anaee[2,3], Ahmed M. Al-Ghaban[2], Hussain M. Yousif[4]*

[1]Ministry of Transportation, Iraq
[2]College of Materials Eng., University of Technology- Iraq
[3]Nanotechnology and Advanced Materials Researches Center, University of Technology- Iraq
[4]State Company for Steel Industries, Ministry of Industry and Minerals, Iraq
[*)] Email: mae.22.038@grad.uotechnology.edu.iq

Received 10/7/2026, *Received in revised form* 24/8/2026, *Accepted* 5/9/2026, *Published* 15/10/2026

In this study, a novel technique is developed to enhance the corrosion resistance of steel rebars by spraying-by-spraying metallic nanopowders of zinc and tin onto the surface of hot-rolled steel. After embedding in a concrete mixture, the coated and uncoated steel samples are immersed in a 3.5% NaCl solution for 28, 56, and 90 days at various temperatures (298, 308, and 318 K). Surface morphology and structural characterization are investigated using scanning electron microscopy (SEM), atomic force microscopy (AFM), and X-ray diffraction (XRD), confirming the formation of uniform, dense coatings with fine-grained crystallinity. The zinc coating exhibited a surface roughness of 18.82 nm and a mean particle diameter of 87.71 nm, while the tin coating achieved an even more compact structure with a surface roughness of 8.141 nm and a finer particle diameter of 33.15 nm. Electrochemical tests revealed that the best corrosion protection is achieved by the tin-coated steel, with a maximum inhibition efficiency of 96.53% at 298 K after 28 days, followed closely by the zinc-coated sample at 96.47% under the same conditions. Electrochemical impedance spectroscopy (EIS) analysis revealed that the highest solution resistance (15,129$\Omega.cm^2$) and Warburg impedance (26,632 $\Omega.cm^2$) are for the tin-coated sample at 298 K after 56 days, while Zn-coated samples recorded values of (11,897$\Omega\cdot cm^2$) and (5.432×1015 $\Omega\cdot cm^2$), respectively. These findings confirm the effectiveness of the proposed coating method in significantly improving corrosion resistance and service life of reinforced concrete structures in chloride-contaminated environments.

Keywords: Tin; Zinc; Coating; NaCl Solution; Corrosion.

1. INTRODUCTION

Concrete is the most commonly used construction material due to its preference in applications requiring permanence and strength. Consequently, the corrosion of steel-reinforced concrete is a major factor in reducing the service life and durability of reinforced concrete buildings. One of the primary causes of corrosion is chloride ions intrusion, which compromises the passive layer on steel reinforcement and initiates localized corrosion. This leads to the accumulation of corrosion products, resulting in concrete delamination and cracking. As a result, the load-bearing capacity of reinforced concrete structures is significantly weakened. The widespread deterioration of these structures due to localized steel corrosion causes substantial damage, making steel protection and corrosion prevention in concrete a critical concern [1-5].

Many techniques have been used to improve the performance of reinforced concrete, focusing either on the mortar itself through the incorporation of micro- and/or nano-additives [6–9] or on creating an environment that protects the steel reinforcement by promoting the formation of a passive layer. On the other hand, different techniques are used to slow-down or prevent the corrosion of steel-rebars in concrete, including inhibitors, sacrificial anodes, impressed currents and coatings. Numerous research studies have shown that applying protective materials, particularly metallic coatings on steel rebars, significantly reduces chloride ion penetration by hindering their diffusion into the steel, thereby extending its service life. However, the challenge of this study lies in selecting the type of coating material and the method of application, as they determine important factors such as cost and performance [10].

The hot-rolling process is considered the most critical step in the manufacturing of reinforcing steel bars. This process involves heating the steel to high temperatures and then passing it through rolling mills to achieve the desired cylindrical shape and dimensions. Hot rolling not only ensures the uniformity of the steel, but also improves its mechanical properties. In the present study, the thermal conditions associated with the hot-rolling process are utilized to facilitate the application of protective metallic coatings during steel manufacturing.

Many studies are conducted regarding preventing the corrosion of carbon steel placed in cement past through different coating techniques. Cedrim et al. [11] have evaluated the corrosion resistance of electroplated Zn and Zn/Ni coatings on steel rebars in concrete. Salt spray and wetting/drying cycles in NaCl solution are used to accelerate corrosion, with weight loss as the evaluation metric. Nguyen et al. [12] have investigated the application of epoxy coatings with nano-Fe_2O_3 and nano-SiO_2 on reinforcing steel bars in chloride-contaminated cement mortar (0.3% and 0.5% NaCl). Muazzam et al. [13] have assessed the two-year corrosion behavior of bare and epoxy-coated steel rebars in chloride-rich concrete, the results revealed that the epoxy coated bar showed no corrosion deterioration, and exhibited very high charge transfer resistance. While Arkadeb and Sarmila [14] have studied the corrosion performance of electroless-Ni coatings (Ni-P, Ni-P-Cu and Ni-P-W,) on steel reinforcement bars in (3.5% NaCl). Alireza et al. [15] have incorporated pozzolanic materials and 2-dimethylaminoethanol into concrete to reduce rebar corrosion. Different steels are treated with various primer systems. Meanwhile, Muazzam et al. [16] have examined the corrosion resistance of different coated and uncoated steel rebars under harsh climatic conditions over 16 months. Abdulaziz et al. [17] have enhanced the behavior of galvanized steel rebars when imbedded in a chloride contaminated concrete, by alloying zinc with different percentages of aluminum. Ebrahimi et al. [18] have applied by plasma spraying, bi-layer HA/Al_2O_3-SiO_2 coatings (10–30 wt% SiO_2) on Ti surfaces exhibited greater roughness with more layers. Corrosion resistance peaked at 20% SiO_2. Arda et al. [19] have employed the thermionic vacuum arc method to deposit Zinc, Zinc-Boron, and Zinc/Boron-Nitrogen nanoparticle coatings on steel reinforcement. Chandra et al. [20] have used alkali activated slag coatings to prevent

the corrosion of rebars in a marine environment. The coatings, both with and without the modification of latex-polymer, are compared to a conventional-cement coating. Hao Qian et al. [21] have studied the behavior of enamel coatings on reinforcing steel in resisting corrosion, focusing on SiC content (2.5%, 5%, 7.5%) and microstructure over 210 days. Saniee et al. [22] have applied via CAE-PVD, CrN/CrAlN nanolayered coatings. The outcomes improved corrosion potential, reduced current density, and acted as effective barriers against corrosive media. Susetyo et al. [23] have employed a rotating barrel system to deposit Ni-films on a metallic-substrate at varying speeds (0–100 rpm). Increasing the barrel speed reduced deposition parameters and improved corrosion resistance. Petr Pokorn et al. [24] have used a plasma-sprayed Al_2O_3coating topped with Zr-based and organo-silane coatings to protect reinforced steel. The combined topcoats boosted corrosion resistance. On the other hand, Hao Peng et al. [25] have studied the effects of incorporating additives on the corrosion performance of polymer-cement composite coatings. The optimal formulation (45 wt% emulsion, 6 wt% pigment filler, 0.3 wt% dispersant) significantly enhanced bonding to rebars, and thereby improved corrosion resistance.

This study aims to use nano-particles of zinc and tin as individual barrier coatings to protect steel reinforcement bars in concrete structures from accelerated corrosion. The innovative method involves spraying Zn-nano-powder after the hot rolling process of steel rebar, while the rebar remains sufficiently hot to ensure strong adhesion and durability of the coating layer; the same procedure is applied to Sn-nano-powder. The performance of the coated steel is evaluated by immersing the samples for three different durations in a 3.5 % NaCl solution to simulate seawater conditions.

2. METHODOLOGY

2.1. Materials

2.1.1. Cement

Sulphate-resisting Portland cement (SRPC) produced by the Lafarge cement factory is used in the concrete mixture. The chemical contents of SRPC are (63.6% CaO, 3.98% Al2O3, 19.35% SiO_2, 3.32% MgO, 5.03% Fe_2O_3, 1.71% SO_3, 0.02% Cl, 0.4% C_2S, 72.99% C_3S, 2.05% C_3A, 15.31% C_4AF, 1.1% I.R, and 3.05% L.O.I.), that are in accordance to the limits of Iraqi specifications No. 5/2019 [26].

2.1.2. Fine aggregate

Sand containing 0.4%SO_3, according to the Iraqi standard specifications No.45 in 1984 [27], is supplied from the quarries of Karbala governorate to be used in all concrete mixes.

2.1.3. Coarse aggregates

Black-crushed gravel of 10 mm maximum size, conforming to the Iraqi specification limits (No. 45/1984) is used in the study [27].

2.1.4. Reinforcing steel

Steel reinforcing bars manufactured by Mass Iraq for Iron and Steel Industry are used as the substrate material in this study. These rebars comply with the requirements of ISO 6935-2:2015 [28]. The rebars had a diameter of 1.2 cm and a length of 1.3 cm. Their chemical composition is presented in Table 1. The yield strength and tensile strength of the steel are 608 N/mm^2 and 689 N/mm^2, respectively.

Table 1 The chemical composition of carbon steel samples.

C	Si	Mn	P	S	Cr	Ni	Cu	Al
0.22	0.6	1.6	0.05	0.05	0.1	0.1	0.33	0.01

2.1.5. Water

Tap water with a pH value of (7.5) is used in the concrete mixture to produce cubic samples, while salt-water (3.5 % NaCl) is used as aggressive media for different periods of time (28, 56, and 90) days.

2.1.6. Coating

Nano-powders of Zinc (Zn) and tin (Sn), produced by Thomas Baker (Chemicals) Pvt. Ltd. and Sigma-Aldrich companies, respectively, with particle sizes ranging from 20 to 250 nm and a purity of 99.5%, are selected as coating materials for the steel substrate.

3. EXPERIMENTAL PROCEDURES

3.1.Coating process

The current coating technique is designed to save time, effort, and money by coating and manufacturing reinforcing steel bars simultaneously. It simulates the temperature of the "hot rolling process" using a stainless-steel cylindrical induction furnace (see Figure 1), which is enclosed by two discs. One disc has openings for inserting the steel bar to be coated and a thermocouple to monitor temperature, while the other disc has two aligned nozzles above and below the rebar through which the metal powder is sprayed onto the hot surface of steel bar.

Two types of nanometallic coatings are used: zinc and tin, each is applied individually. During zinc plating, the rebar intended for coating is placed inside the furnace chamber and heated to the melting point of zinc (400-440°C). The zinc powder is then injected through the nozzles at 116 bar. The zinc melts on contact, forming a uniform protective coating on the entire surface of the specimen, with a thickness ranging from (4 to 8) microns. The same process is followed for tin plating, where the rebar is heated to the melting-point of tin (200-220°C). A total of (18) reinforcing bar specimens are coated with each coating type.

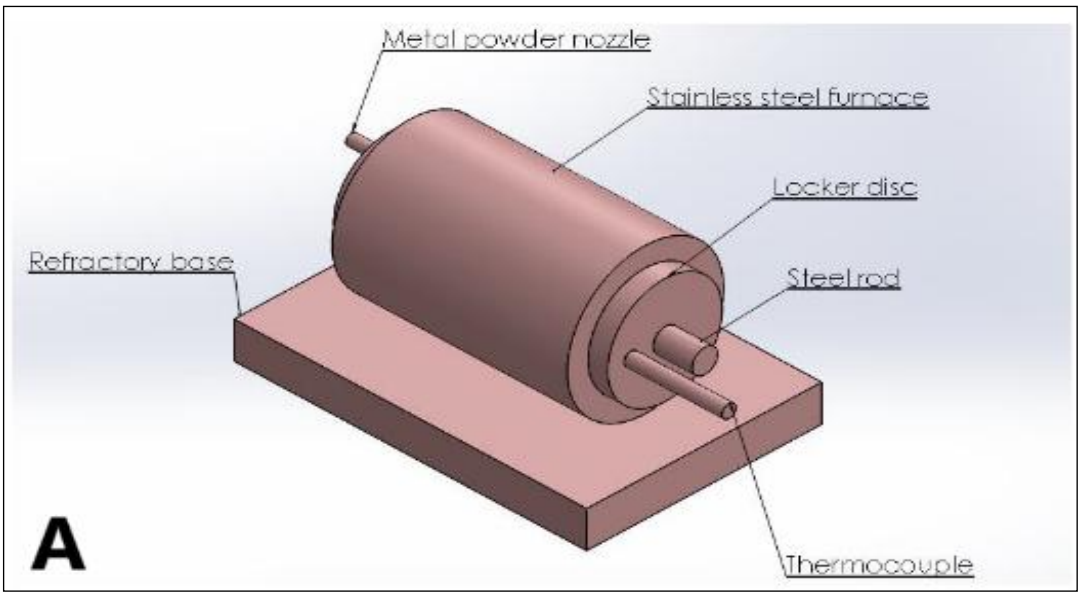

Figure 1 A schematic of the Cylindrical Induction Furnace.

Then coated reinforcing bars are subsequently bent to an angle of 90°, according to the procedure in reference [29], to simulate mechanical stresses that might occur in real-life conditions. After bending, the samples are visually inspected for cracking, peeling or flaking. No coating damage is observed, and the coating layer remained continuous and firmly adhered to the steel substrate, indicating excellent mechanical integrity and adhesion.

3.2.Concrete sample preparation

The mixing process is carried out using an electric mixer with a 50L capacity. The concrete components are added in a sequence: cement is placed over the sand and gravel. The dry materials are thoroughly mixed for two minutes to ensure uniform distribution. Subsequently, water is gradually introduced into the dry mixture, and mixing continued for an additional three minutes to achieve homogeneous and consistent mixture. Table 2 showing the amounts of concrete mixture.

Table 2 The measured components of the concrete mix.

Fcu (28 days) Mpa	Cement (Kg/m^3)	Sand (Kg/m^3)	Gravel (Kg/m^3)	Water (L/m^3)
30	310	720	1190	154.5

The coated-reinforcing bars are positioned vertically inside cubic molds (10×10×10 cm) using 2.0 cm spacers. The concrete mixture is then poured into the molds, which are placed on a vibrating table to eliminate air bubbles and ensure proper compaction. After 48 hrs of casting, the concrete samples are demolded and submerged in tap water for 28 days to cure. Subsequently the reinforced concrete cubes are immersed in seawater (3.5 wt.% sodium chloride) for varying durations (28, 56, and 90 days) to assess the corrosion behavior and resistance to chloride attack.

3.3.Measurements

For characterization of the coated surface, X-ray diffraction (XRD), Scanning electron microscopy with energy-dispersive spectroscopy (SEM/EDS), and atomic force microscopy (AFM) are employed. The structural properties of the applied coating are analyzed using XRD (Shimadzu, Japan) with a

scanning rate of 1° min^{-1} over an angular range of 10° to 90°. Surface morphology and elemental composition are examined using SEM equipped with EDS (Thermo Fisher scientific company, USA). Finally, surface topography and roughness are assessed through high-resolution imaging with an atomic force microscope (FlexAFM-Axiom, Nanosurf AG, Switzerland).

3.4. Corrosion

Electrochemical measurements are conducted using a Corrtest Potentiostat (model: CS350M) with three-electrode cell configuration: (1) The working electrode, which includes the coated and uncoated steel-rebar samples; (2) The reference electrode, which is a saturated calomel electrode (SCE). The tip of the reference electrode is positioned approximately one-millimeter from the surface of the working electrode in the solution to minimize experimental error; (3) An auxiliary electrode made of platinum, positioned directly opposite the working electrode in the electrochemical cell, As reported in Reference [29].

Tafel plots are obtained for uncoated and coated samples, and the data are analyzed using the Tafel extrapolation method to estimate the corrosion-current density (i_{corr}), corrosion-potential (E_{corr}), and Tafel slopes for the anodic (b_a) and cathodic (b_c) sections. Subsequently, polarization resistance, protection efficiency and porosity percentage are determined [30,31]. Additionally, the electrochemical impedance spectroscopy (EIS) is determined to assess the resistance properties of all steel samples. This analysis is conducted through Nyquist plots, which offer valuable insights into solution resistance, charge transfer resistance, and diffusion processes [32].

4. RESULTS AND DISCUSSION

4.1. Characterization of coated surface

XRD analysis is used to characterize the surface of the coated samples, and the resulting diffraction patterns are presented in Figure 2. In Figure 2(a), the main diffraction peaks of the uncoated steel bar are observed at 2θ values of 43.76°, 59.84°, 64.28° and 81.68°, corresponding to the standard steel reference pattern (JCPDS card No. 35-1357). On the other hand, Figure 2(b) shows the primary peaks of the Zn-coated steel bar at 2θ values of 44.68° and 82.28° as identified by JCPDS card No. 01-1238. Additionally, the mixed peaks appearing between 40 and 50° may be attributed to ($FeZn_{8.87}$) phase (JCPDS card No. 45-1185) or the ($FeZn_{10.98}$) phase (JCPDS card No. 45-1184). The temperature during the experiment facilitated the diffusion and incorporation of zinc into the steel surface, while Figure 2(c) reveals only one main peak in the tin-coated rebar at 2θ value of 36.48°, Other observed peaks are close to those associated with the formation of ($FeSn_2$) phase, according to (JCPDS card) No. 25-0415. This indicates that tin has a good ability to diffuse into the upper layer of the steel surface, facilitated by the high temperatures generated during the coating process. This diffusion promotes the formation of a more integrated layer and may also lead to the formation of tin oxide through oxidation.

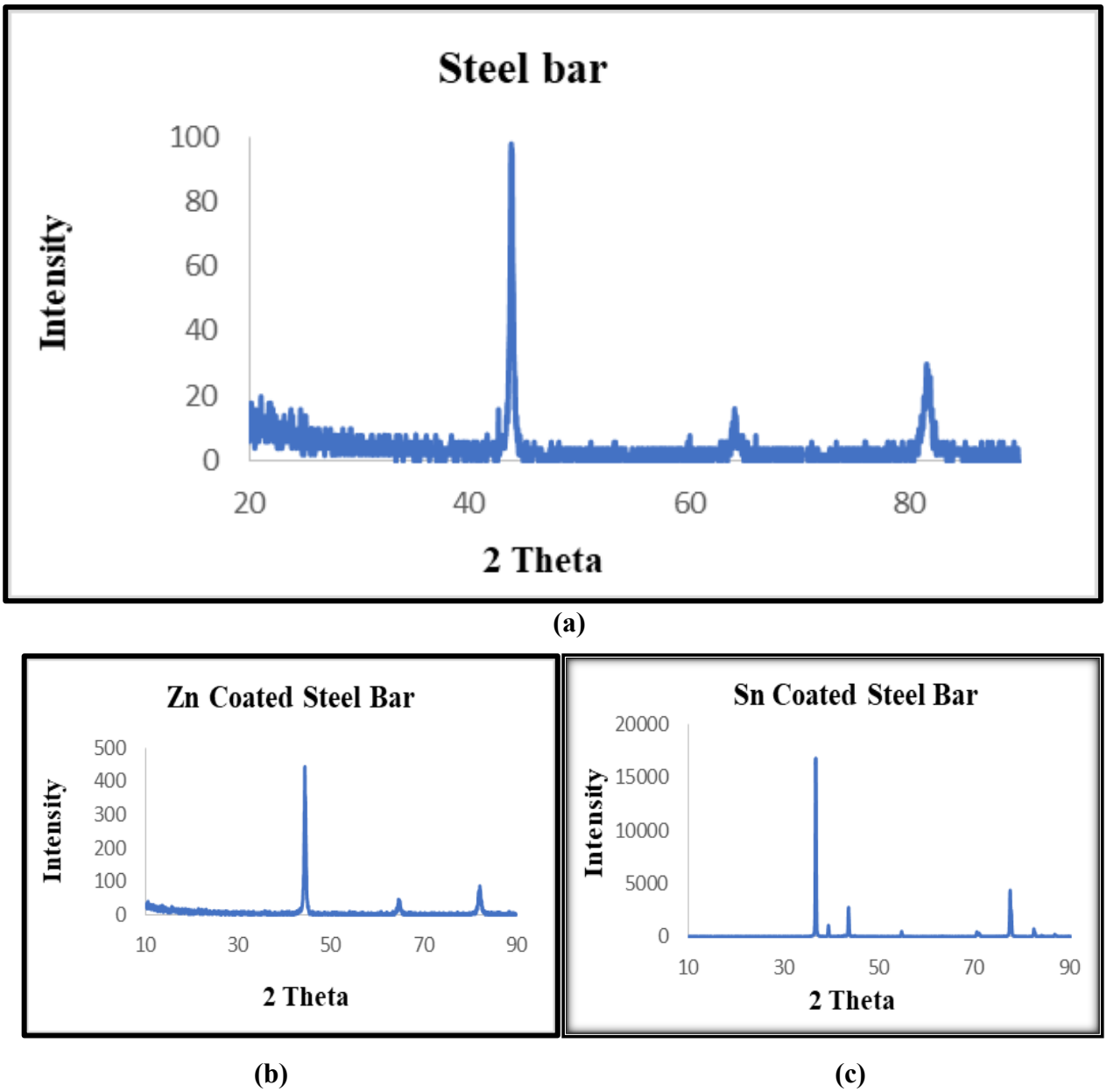

Figure 2 The XRD Pattern of: (a) Steel Bar, (b) Zn-Coated Steel, and (c) Sn-Coated Steel.

Scanning electron microscopy with energy dispersive spectroscopy (SEM/EDS) is also used to characterize the zinc and tin coated steel bars in comparison with the uncoated ones. Figure 3(a) showed the irregular edges associated with the features of steel bars used in construction to enhance adhesion with cement paste, resulting in rough surface. Meanwhile, the elemental composition analysis in Figure 3(b) confirmed the presence of all base elements [33], especially iron (86.7 wt%) as the primary constituent.

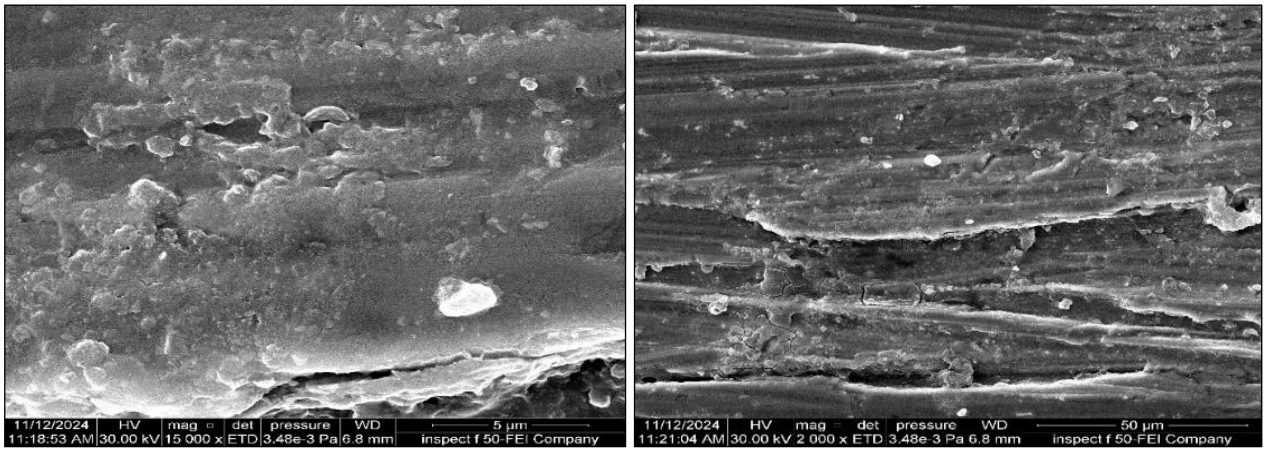

(a)

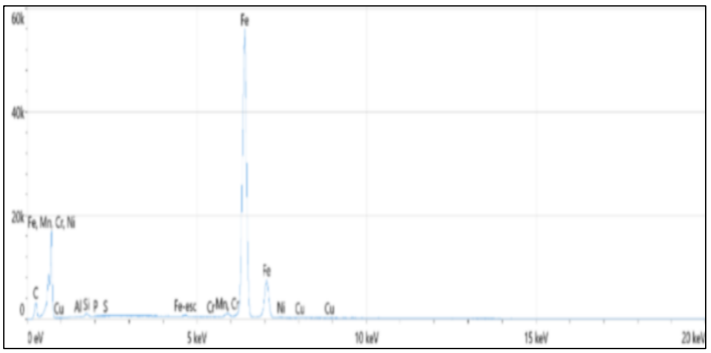

Element	Weight %
Al	0.1
Si	0.5
Mn	1.3
Fe	86.7
Ni	0.3
Cu	0.2
Cr	0.1

(b)

Figure 3 (a) SEM and (b) EDS of Plain Steel-Bar.

As for Zn-coated reinforcement steel, the images in Figure 4(a) reveal that the steel substrate is uniformly covered by zinc particles, resulting in the formation of a homogeneous coating layer with a thickness of 6.44–8.03 µm. The presence of this continuous zinc layer contributed to the cathodic protection of the steel bar. This observation is consistent with the findings of Schaefer and Miszczyk, who demonstrated that zinc-rich paints improved electrochemical protection by ensuring direct contact between spherical zinc particles, thereby maintaining cathodic protection [34]. On the other hand, the EDS analysis in Figure 4(b) confirmed that the zinc is the predominant element, with a content of 69.5%, followed by oxygen at 8.9%, which is attributed to oxidation at elevated temperatures.

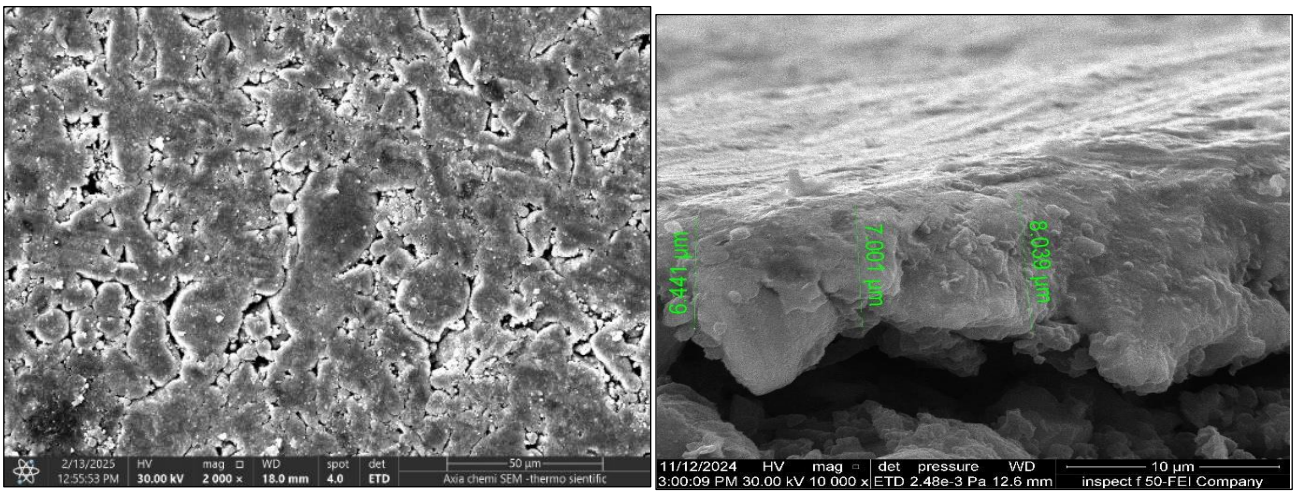

(a)

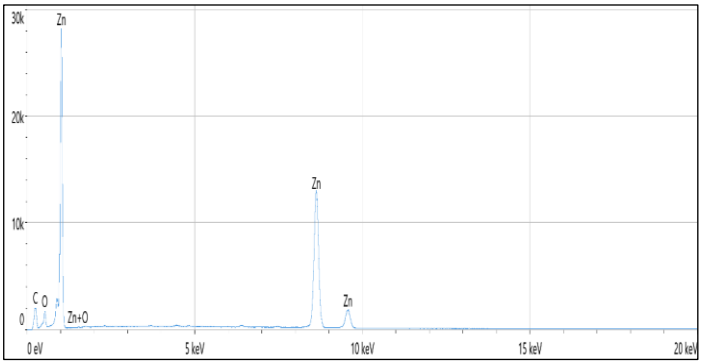

Element	Weight %
O	8.9
Zn	69.5

(b)

Figure 4 (a) SEM and (b) EDS Analysis of Zinc-Coated Steel.

In the case of tin-coated steel reinforcing bars, the SEM images in Figure 5(a) indicate that tin diffused effectively into the steel substrate, forming a dense, compact layer with a thickness of approximately 4µm. This layer significantly enhanced the protective capability of the coating by acting as an effective barrier against the penetration of aggressive agents [35]. Meanwhile, the EDS analysis in Figure 5(b) revealed the presence of 58.1% tin, in addition to the presence of iron and oxygen. These detected elements confirm the phases suggested by the XRD analysis.

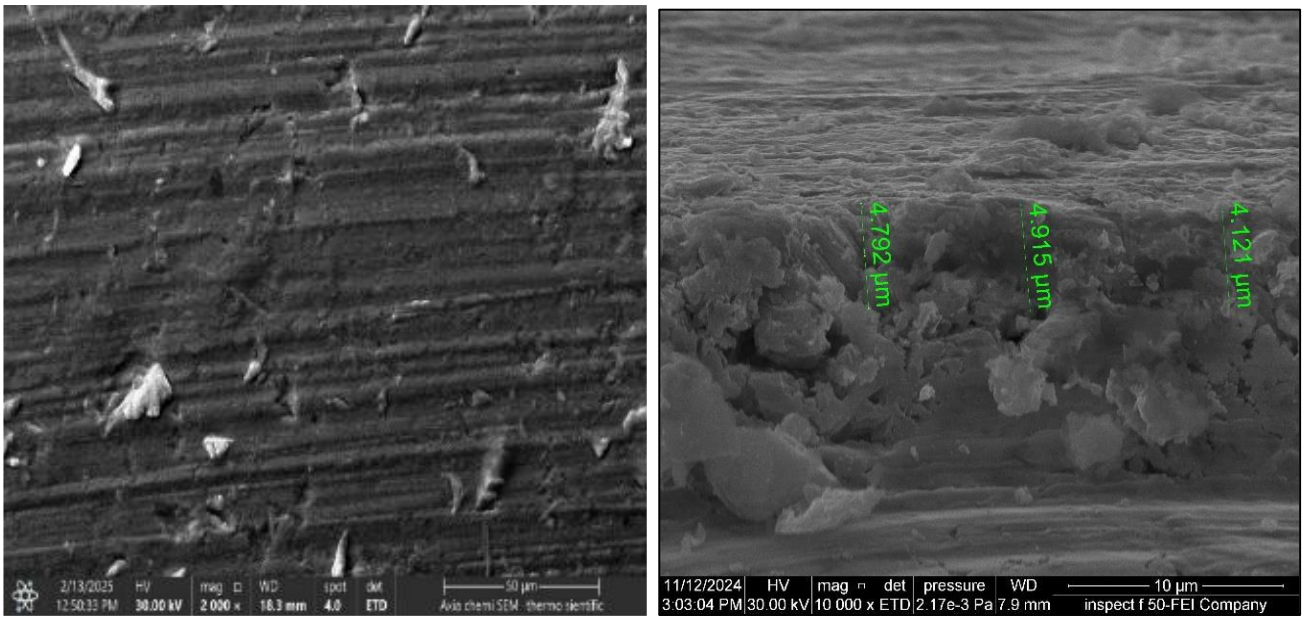

(a)

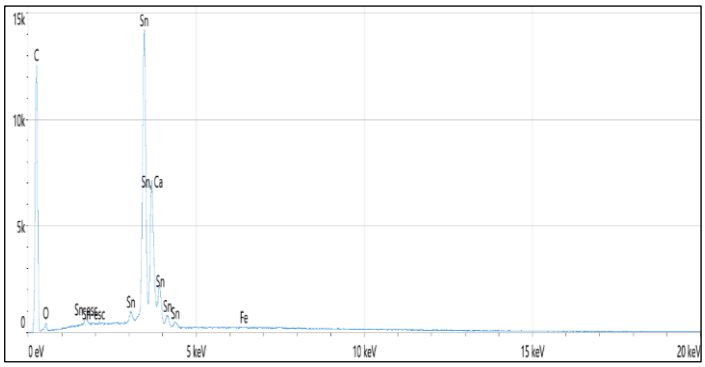

Element	Weight %
O	4.8
Ca	0.7
Fe	0.2
Sn	58.1

(b)

Figure 5 (a) SEM Images and (b) EDS Results of Sn-Coated Steel Bar.

Atomic force microscopy (AFM) is employed to examine the surface topography of Zn and Sn coated rebars, as well as the uncoated ones by measuring its surface roughness, and particle size. It is also used to estimate the value of the adhesion force between the probe of the cantilever and the surface of the coated sample, as illustrated in Figures 6 to 11. In Figure 6, the images are presented in two and three dimensions, highlighting the valley-like features of the surface. These surface characteristics are essential for ensuring proper bonding between the reinforced steel bar and the cement paste, resulting in a high surface roughness of 133.6 nm.

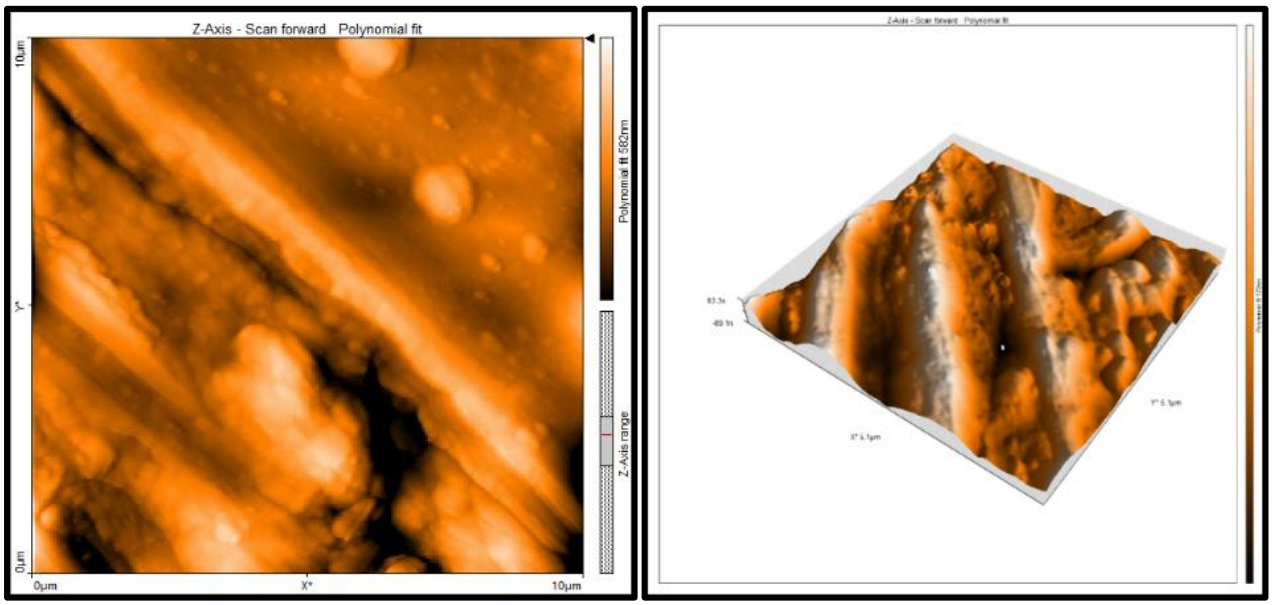

Figure 6 AFM of Steel Bar.

On the other hand, the images of the Zn-coated steel surface in Figure 7, reveal isolated and segregated structures. Various phases can form between Zn and Fe, including the δ ($FeZn_7$) phase when iron solubility in zinc is below 0.001%, and the ζ ($FeZn_{13}$) phase, which is a thermodynamically unstable, and others. Therefore, identifying the specific formed phase or achieving compact layer is challenging [36]. These different formed structures gave surface roughness equal to 18.82 nm.

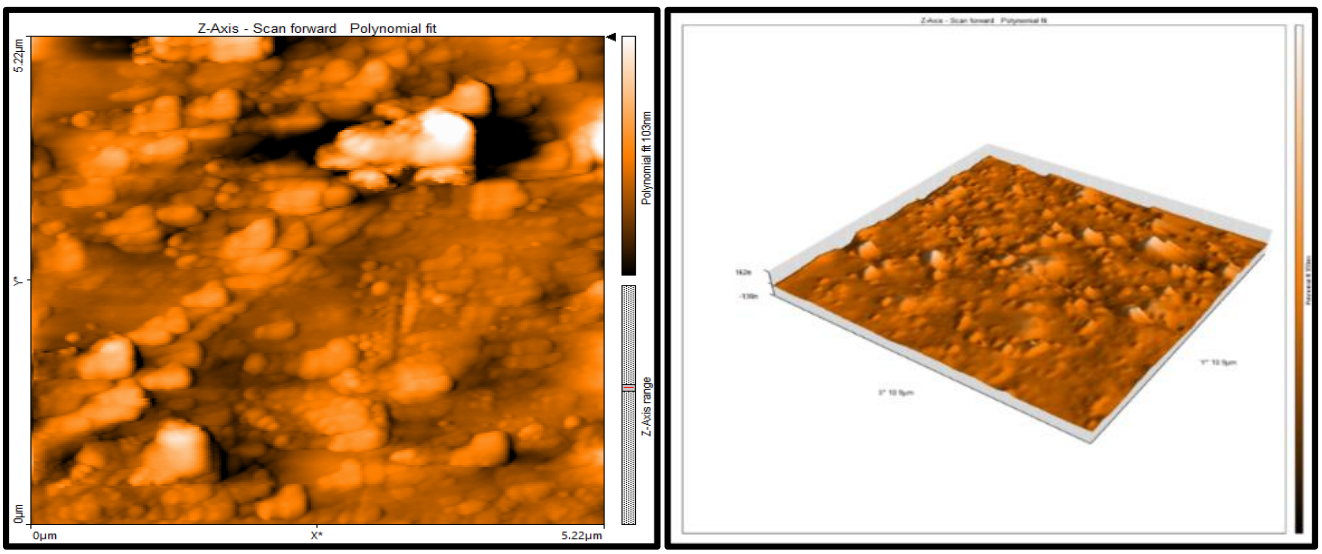

Figure 7 AFM of Steel Coated with Zinc.

The force–distance curve of the reinforcing bar coated by zinc reveals a moderate adhesion force of -1.517 nN, in addition to a Young's modulus of 1.549 MPa, as demonstrated in Figure 8. This behavior may be attributed to the formation of intermetallic phases between iron and zinc (FeZn7, FeZn13), which leads to a strong metallurgical bond at the interface [37].

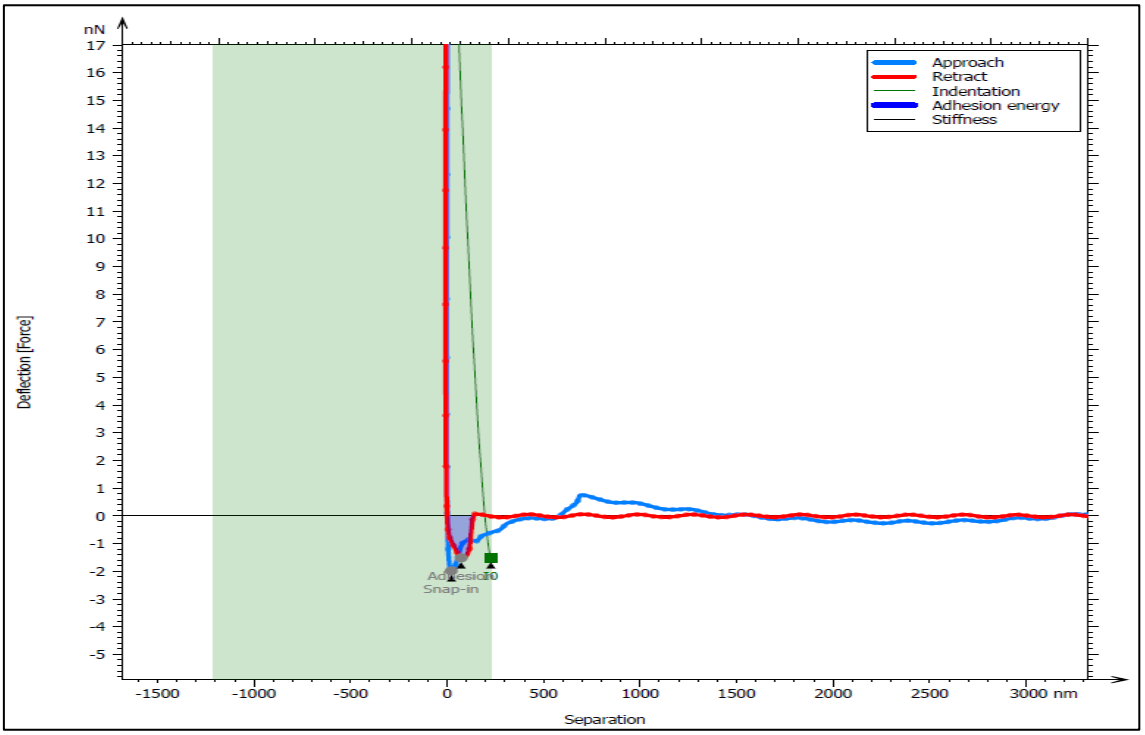

Figure 8 The adhesion force curve for Zn-sample.

As for the steel bars coated by tin, the inspection by AFM gave the images shown in Figure 9, revealing a mixture layer of multi-phase cores, which is also observed by Yong et al. when they precipitated (Sn/ $FeSn_2$/FeO) by and thermal reduction treatment. They obtained a novel yolk-shell nanostructure with multi-phase nanocores consist of Sn, $FeSn_2$and FeO nanoparticles [38]. A surface roughness of 8.141 nm is recorded, confirming the formation of a dense coating layer on the steel surface.

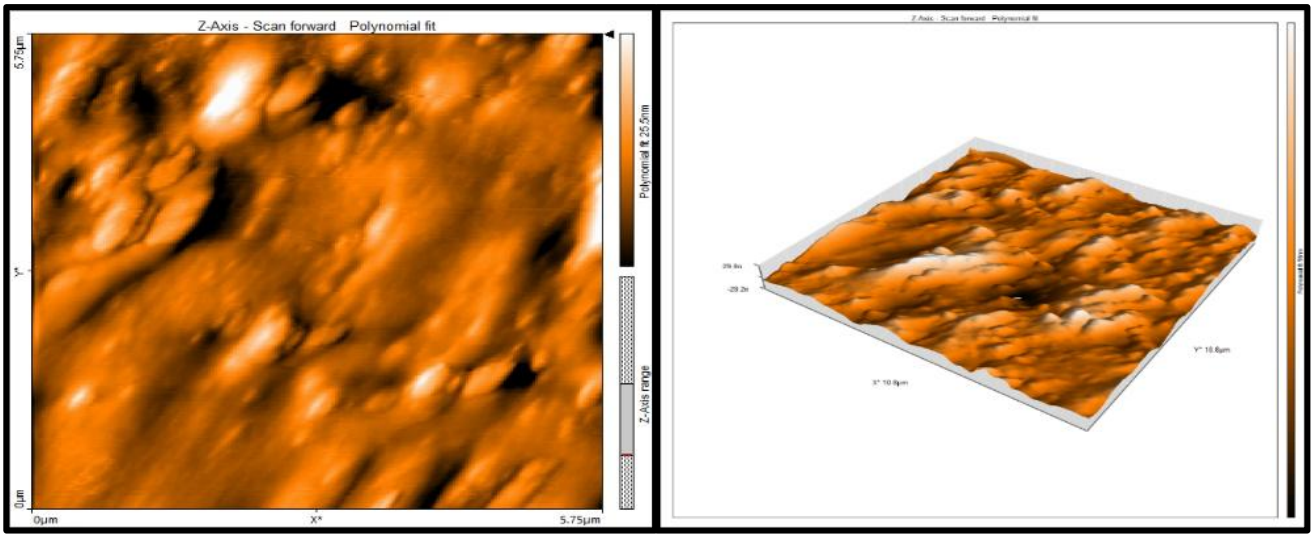

Figure 9 AFM Images of Tin-Coated Steel Bar.

Sn-coated steel sample expresses a moderate adhesion force of -1.75 nN and Young's modulus of 2.062 MPa, as indicated in Figure 10. The presence of oxide compounds (FeO, $FeSn_2$) plays an important role in anchoring the tin coating layer to the steel substrate.

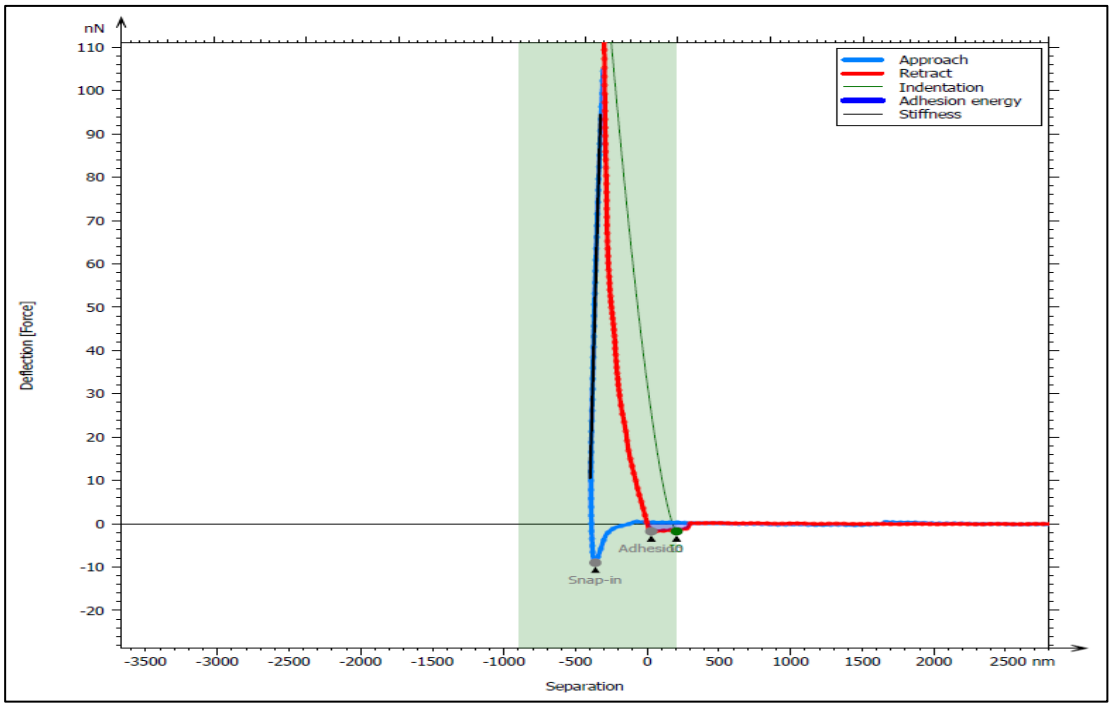

Figure 10 Deflection-Separation curve of a sample with Sn-coating.

The particle distribution chart for the steel bar and the coated ones can be seen in Figure 11. It shows that the highest area for medium particles obtains a mean diameter of 195.7 nm for the steel bar, whereas, in the case of steel coated with Zn, the highest area is for small particles, resulting in a mean diameter of 87.71 nm, while a small mean particle diameter of 33.15 nm is determined for tin-coated steel bars. This decrease in mean diameter after coating confirms the reduction in corrosion risk due to

full coverage by zinc and tin atoms, along with the formation of ($FeZn_{8.87}$ or $FeZn_{10.98}$) phase. From the data of AFM scan, the number of particles is recoded as 125, 512, and 439 for the uncoated steel, zinc-coated, and tin-coated steel surfaces respectively, with a particle density of 13,786,312 Particles/mm^2, 18,807,456 Particles/mm^2, and 41,897,151 Particles/mm^2 respectively. This increase in particles and density may attributed to the formation of a denser, more compact surface layer after coating.

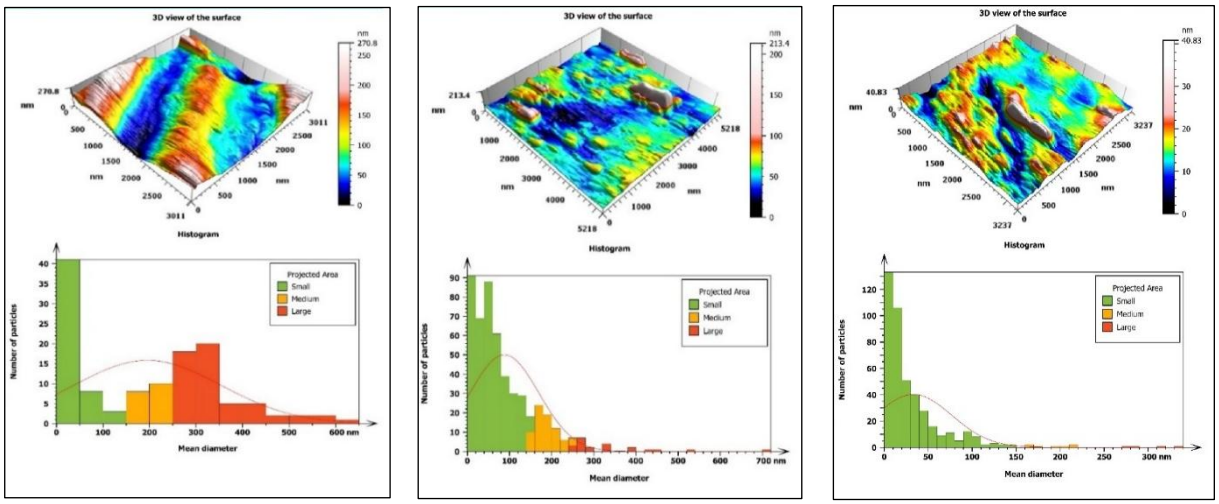

(a) **(b)** **(c)**

Figure 11 Particle Distribution Charts for: (a) Uncoated Steel Bar, (b) Zn-Coated Bar, and (c) Sn-Coated Bar.

4.2. Corrosion behavior

The primary goal of this study is to minimize the risk of corrosion, as determined from recorded polarization curves. Figures 12 to 14 illustrate the Tafel plots for both uncoated and coated steel bars after three different immersion periods (28, 56, and 90 days) in sea-water. In general, the corrosion potential of the steel bars varies with immersion time, while the corrosion current tends to increase as immersion time extends. This is due to prolonged exposure to aggressive species that penetrate the cement paste, eventually reaching the steel surface and breaking down the passive film through chemical reactions [39]. The anodic process releases Fe^{2+} cations [40]:

$$Fe \rightarrow Fe^{2+} + 2e^- \quad (1)$$

The corresponding cathodic reaction, where the O_2 or H_2O reduction take place, produces $2OH^-$ ions by consuming 4 electrons:

$$O_2 + 2H_2O + 4e^- \rightarrow 4OH^- \quad (2)$$

$$2H_2O + 2e^- \rightarrow H_2 + 2OH^- \quad (3)$$

The hydroxyl ions react with Fe^{2+} ions, leading to the formation of ferrous hydroxide:

$$Fe^{2+} + 2OH^- \rightarrow Fe(OH)_2 \quad (4)$$

As ferrous hydroxide interacts with oxygen and water, it converts into $Fe(OH)_3$, forming a protective layer that restricts ion movement within the solution:

$$4Fe(OH)_2 + 2H_2O + O_2 \rightarrow 4Fe(OH)_3 \quad (5)$$

A high concentration of chloride ions in the aqueous adlayer on the metal surface promotes the formation of ferrous chloride ($FeCl_2$), which subsequently hydrolyzes in water:

$$FeCl_2 + 2H_2O \rightarrow Fe(OH)_2 + 2H^+ + 2Cl^- \quad (6)$$

$$3Fe_3O_4 + 9/2\ H_2O + 3/4\ O_2 \rightarrow 9FeOOH \quad (7)$$

The presence of H^+ ions and Cl^- leads to the formation free acid, significantly lowering the pH value around the steel rebar. The above mechanism is self-generative and, once initiated, continues. The increase in the dissolution rate at the anode accelerates the migration of chloride ions, making the reaction time-dependent and continues. This leads to the formation of increasing amounts of $FeCl_2$ and, consequently, the generation of more HCl through hydrolysis. The process persists until the metal is perforated. This attack mechanism is sustained by corrosion products and it is often referred to as referred to as autocatalytic-process [41]. The Tafel slopes (b_a and b_c) and the corrosion current density (i_{corr}) can be used to calculate the polarization resistance (R_p) using the following equation. [42,43]:

$$R_p = \frac{b_c \times b_a}{2.303 \times i_{corr}\,(b_c + b_a)} \tag{8}$$

Coating steel reinforcing bars with zinc and tin using the modified hot-rolling process enhances their durability by forming a barrier that prevents corrosive elements from reaching the substrate, and hence providing corrosion protection [44]. Polarization measurements, as demonstrated in the polarization curves and data presented in Tables 3 to 5, show a clear shift in polarization toward lower current densities after coating, compared to the polarization of uncoated steel. Notably, coating with Sn exhibits more positive corrosion potentials (E_{corr}), whereas the Zn coating shows more negative potential. This is likely due to the standard oxidation potential of Zn (-0.76 V), which is relatively negative and places it at the bottom of galvanic series, making it suitable as a sacrificial anode in cathodic protection. Thus, the bar's resistance to corrosion is increased and the protection efficiency (PE%) is enhanced. The latter is calculated using the corrosion current density of the coated ($i_{corr,coated}$) and uncoated ($i_{corr,uncoated}$) specimens as follows [45]:

$$PE\ (\%) = \left[1 - \frac{i_{corr,coated\ steel}}{i_{corr,uncoated\ steel}}\right] \times 100 \tag{9}$$

The analysis of the PE% data, reveals that the zinc and tin coatings perform optimally at the lowest temperature (298 K), with efficiency decreasing as the temperature increases. The presence of zinc coating on the steel surface facilitates the formation of zinc oxides (ZnO) and zinc hydroxides ($Zn(OH_2)$) when exposed to the electrolyte (Seawater); as described in Equations (10) to (12). These findings, formed due to increased oxygenation in concrete are critical for predicting the lifespan and the progression of the mechanical properties of reinforced concrete structures over time [46].

$$Zn + 2OH^- \rightarrow ZnO + H_2O + 2e^- \tag{10}$$

$$ZnO + H_2O + 2OH^- \rightarrow [Zn(OH)_4]^{2-} \tag{11}$$

$$[Zn(OH)_4]^{2-} \rightarrow Zn(OH)_2 + 2OH^- \tag{12}$$

For tin, the rust layer forms as a result of anodic reaction products. The corrosion resistance of this layer is enhanced when tin-coating is applied to the steel surface. The Sn element can form corrosion-resistant compounds, such as SnO and SnO_2, which improve the layer's performance. Furthermore, the coprecipitation of tin and iron oxides contributes to a more uniform and compact structure. The possible oxidation reactions of tin are explained as follows [47]:

$$Sn + 2OH^- + 2e^- \rightarrow Sn(OH)_2 \tag{13}$$

$$Sn + 2OH^- + 2e^- \rightarrow SnO + H_2O \tag{14}$$

$$Sn(OH)_2 + 2OH^- + 2e^- \rightarrow Sn(OH)_4 \tag{15}$$

$$SnO + H_2O + 2OH^- + 2e^- \rightarrow Sn(OH)_4 \tag{16}$$

Within the rust layer, $Sn(OH)_2$ and $Sn(OH)_4$ compounds are unstable and tend to transform into the more stable forms of tin oxides, namely SnO and SnO_2, as demonstrated below:

$$Sn(OH)_2 \rightarrow SnO + H_2O \tag{17}$$

$$Sn(OH)_4 \rightarrow SnO_2 + 2H_2O \tag{18}$$

In addition, the porosity percentage (PP%), can be determined as follow [47]:

$$PP\% = \frac{R_{p,\ \text{uncoated steel}}}{R_{p,\ \text{coated steel}}}\ 10^{\frac{-\Delta E_{corr}}{b_a}} \times 100 \tag{19}$$

where $R_{p,\ uncoated}$ and $R_{p,\ coated,}$ represent the polarization resistance values for the uncoated and the coated specimens, respectively. The term ΔE denotes the difference in corrosion potential between the two, and b_a refers to the anodic Tafel slope associated with the uncoated specimen. The data in Table 6 demonstrated that the porosity of zinc coatings increased with time and temperature, while tin coatings maintained low porosity initially but gradually degraded with extended exposure.

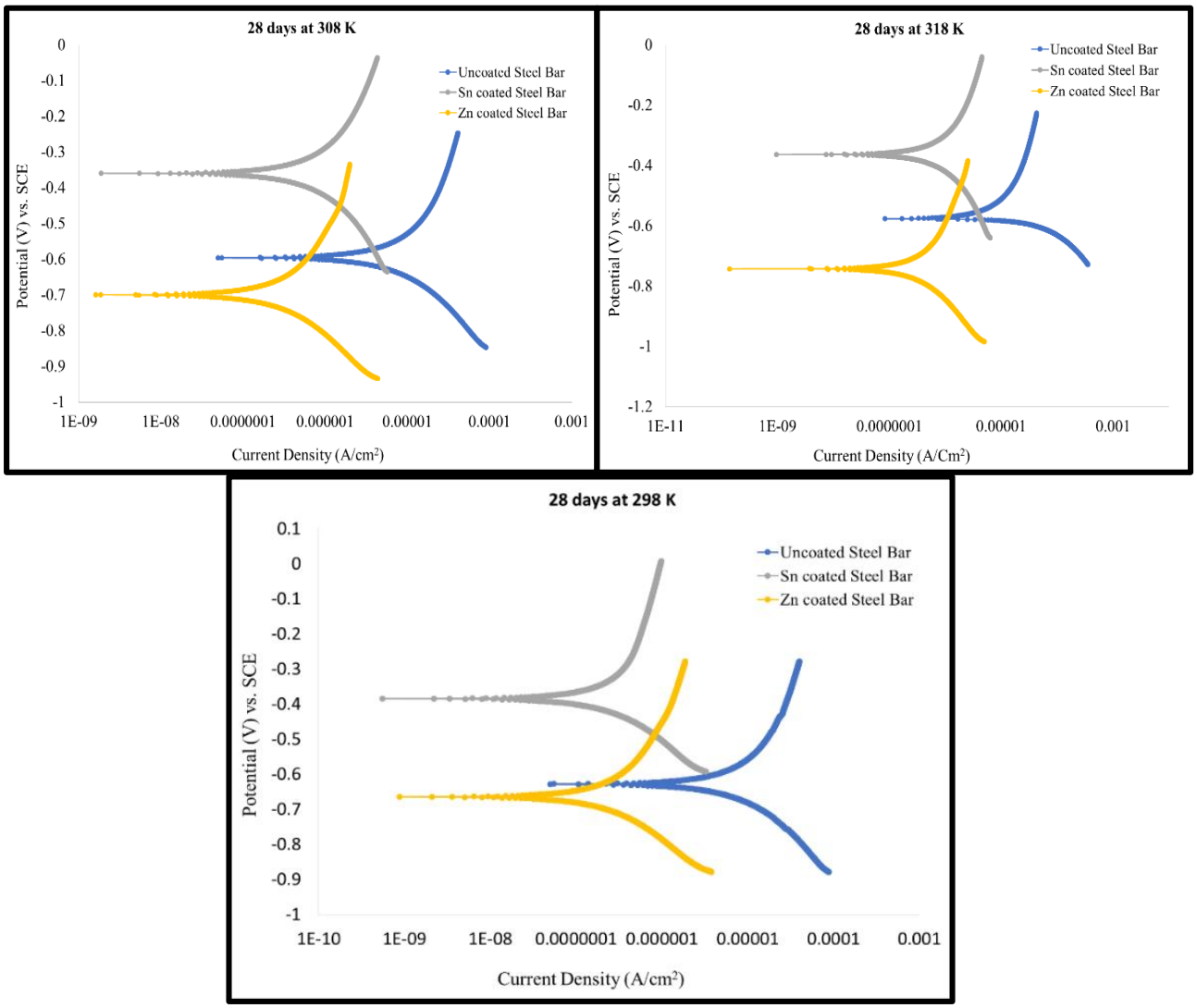

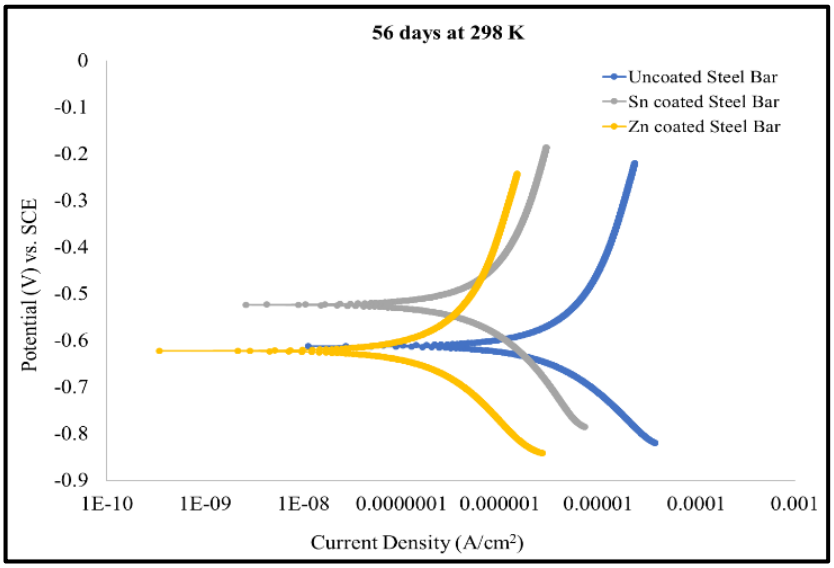

Figure 12 Tafel Plots After 28-Days of Immersion at Three Temperatures.

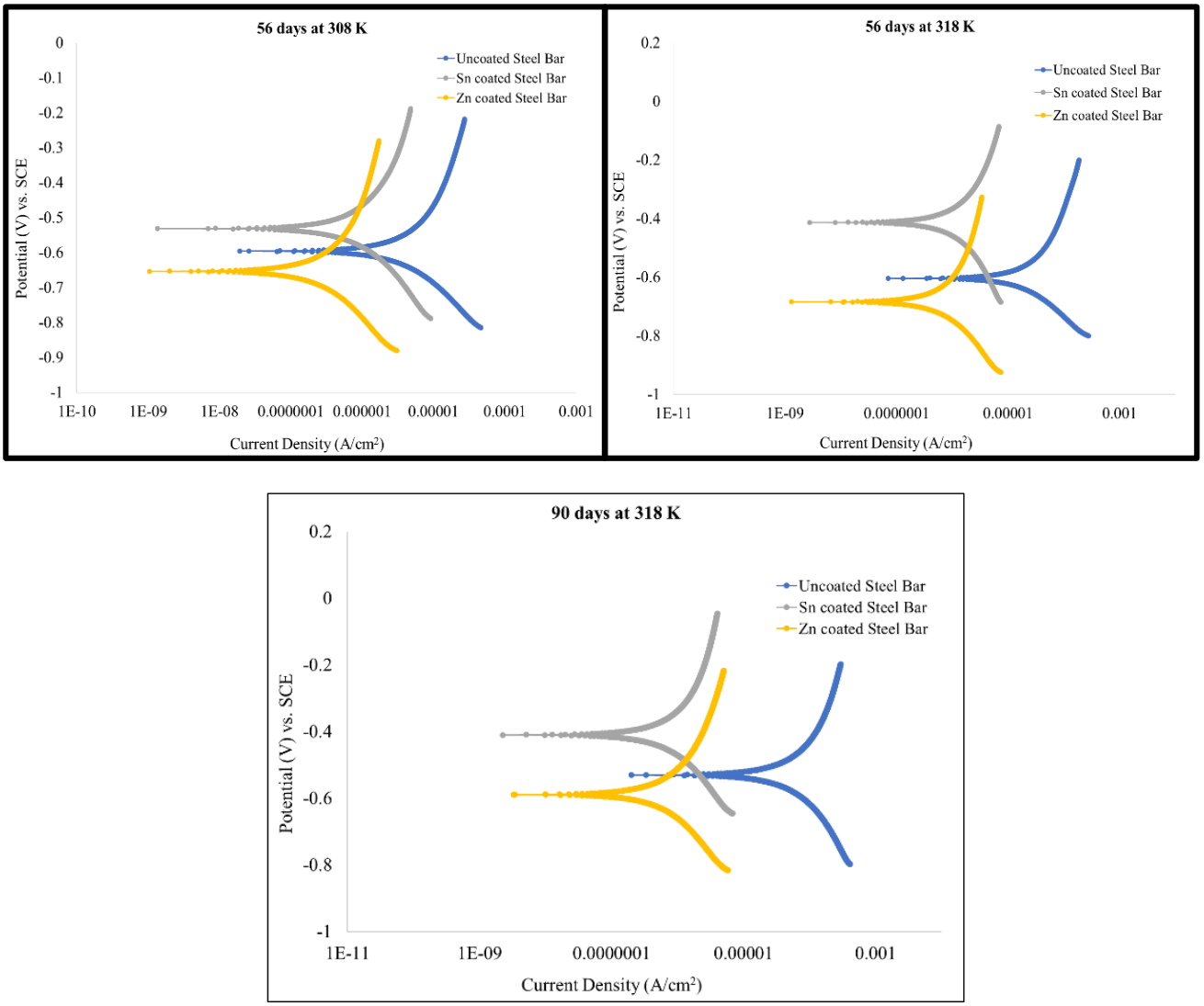

Figure 13 Tafel Curves After Immersion Period of 56 Days at Three Various Temperatures.

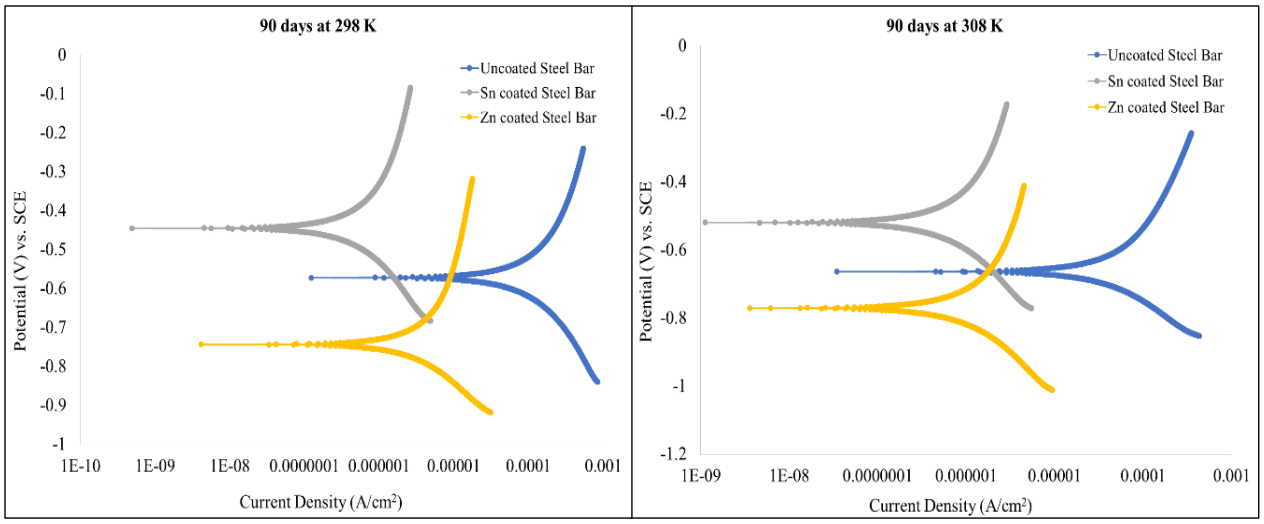

Figure 14 Tafel Plots for Immersion Time of 90 Days at Varying-Temperatures.

Table 3 Corrosion data for uncoated and coated steel bar after immersion time of 28 days at different temperatures.

Coating type	Temp. (K)	$-E_{corr}$ (V)	i_{corr}x10^{-7} ($A.cm^{-2}$)	$-b_c$ ($mV.dec^{-1}$)	$+b_a$ ($mV.dec^{-1}$)	PE (%)	$R_p\times 10^{+4}$ ($\Omega.cm^2$)
Uncoated	298	0.628	14.4	40.727	39.864	-	0.608
	308	0.595	16.26	41.71	21.4	-	0.378
	318	0.576	18.415	37.92	25.58	-	0.360
Zn	298	0.664	0.508	36.305	45.294	96.47	17.247
	308	0.699	3.450	39.606	46.525	78.78	2.696
	318	0.742	4.681	37.032	41.105	74.58	1.809
Sn	298	0.384	0.499	36.981	45.294	96.53	17.738
	308	0.359	2.054	44.854	56.591	87.36	5.296
	318	0.363	3.589	33.26	41.5	80.51	2.236

Table 4 Corrosion data for uncoated and coated steel bar after immersion time of 56 days at different temperatures.

Coating type	Temp. (K)	$-E_{corr}$ (V)	$i_{corr}x10^{-7}$ ($A.cm^{-2}$)	$-b_c$ ($mV.dec^{-1}$)	$+b_a$ ($mV.dec^{-1}$)	PE (%)	$R_p\times 10^{+4}$ ($\Omega.cm^2$)
Uncoated	298	0.612	15.154	297.92	727.42	-	0.606
	308	0.595	16.682	31.04	38.399	-	0.447
	318	0.604	17.5263	31.622	36.34	-	0.419
Zn	298	0.662	2.225	30.378	38.779	85.31	3.328
	308	0.653	3.099	52.918	50.908	81.42	2.189
	318	0.684	3.931	37.333	41.76	77.57	2.180
Sn	298	0.523	1.072	31.273	40.07	92.92	7.123
	308	0.531	1.337	33.272	40.911	91.98	5.966
	318	0.412	2.408	40.45	45.014	86.26	3.846

Table 5 Corrosion data for uncoated and coated steel bar after immersion time of 90 days at different temperatures.

Coating type	Temp. (K)	$-E_{corr}$ (V)	$i_{corr}x10^{-7}$ ($A.cm^{-2}$)	$-b_c$ ($mV.dec^{-1}$)	$+b_a$ ($mV.dec^{-1}$)	PE (%)	$R_p\times 10^{+4}$ ($\Omega.cm^2$)
Uncoated	298	0.572	17.8285	36.612	49.27	-	0.512
	308	0.664	18.716	276.93	604.79	-	0.441
	318	0.529	19.2937	52.414	59.685	-	0.628
Zn	298	0.743	8.564	31.739	36.664	51.96	0.863
	308	0.771	9.086	49.323	48.841	51.45	0.722
	318	0.588	9.1391	28.553	30.245	52.63	0.698
Sn	298	0.445	7.105	33.463	40.528	60.14	1.121
	308	0.519	8.645	40.748	37.348	53.80	0.980
	318	0.409	9.321	38.558	39.266	51.68	0.907

Table 6 Porosity percentages of zinc and tin coatings at different temperatures and immersion periods.

Coating type	Temp. (K)	PP%		
		28 days	56 days	90 days
Zn	298	28.2	21.33	1.75×10^{5}
	308	1.015×10^{6}	661.48	91.8
	318	6.14×10^{7}	3056.2	876.24
Sn	298	2.60×10^{-6}	6.42	0.12
	308	6.691×10^{-11}	0.161	25.91
	318	7.59×10^{-8}	5.67×10^{-5}	0.68

Electrochemical impedance spectroscopy (EIS), is a critical technique in electrochemical analysis, enables the evaluation of a system's impedance (measured in ohms, Ω) to elucidate charge-transfer, mass-transfer, and diffusion processes. This method also provides insights into material properties affecting conductance, capacitance, and resistance. In this study, EIS is employed to analyze uncoated

and coated steel bars after immersion periods of 28 and 56 days at 298 K. Figure 15 illustrates Nyquist plots for all samples after 28 days of immersion. The semicircular arcs in these plots reveal three key resistances: solution resistance(R_s), charge-transfer resistance (R_{ct}), and Warburg impedance (Z_W), alongside double-layer capacitance (C_{dl}). A larger semicircle diameter correlates with higher (R_{ct}), indicating enhanced corrosion resistance. Notably, the Sn- coated rebar, followed by the Zn-coated rebar, exhibited significantly larger diameters than the uncoated sample, consistent with their superior (R_s) and (R_{ct}) values in Table 7. These findings align with Tafel polarization results. A similar trend is observed after 56-day immersion period; as shown in Figure 16 and Table 8 with the coated specimens demonstrating much higher resistance than the uncoated counterpart, as a result of this difference, the uncoated specimens could not be presented within the same figure. Furthermore, while solution resistance (R_s) decreased with prolonged immersion (56 days vs. 28 days), Warburg resistance (Z_w) increased significantly, and diffusion-dominated processes became more pronounced at the longer duration.

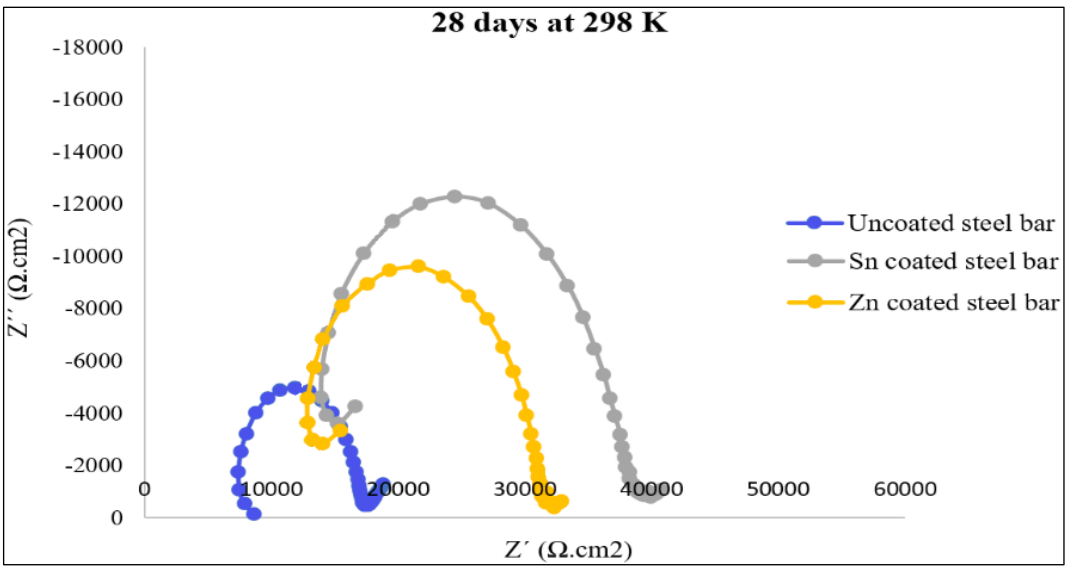

Figure 15 Nyquist Plots for 28 Days Immersion at 298K.

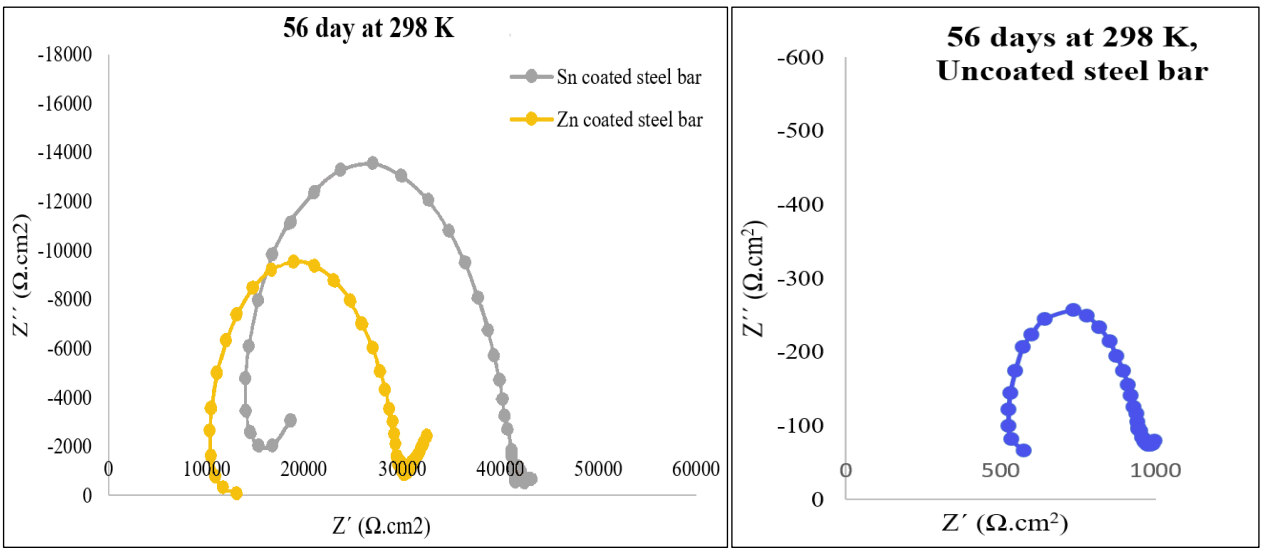

Figure 16 Nyquist Plots for 56 Days Immersion at 298K.

Table 7 The EIS measurements for samples immersed for 28 days at 298 K.

Specimen	R_s (Ω.cm^2)	$R_s + R_{ct}$ (Ω.cm^2)	Z_w (Ω.cm^2)
Uncoated bar	7520	17561	9363
Zn coated bar	14206	31875	75098
Sn coated bar	14881	39708	25256

Table 8 EIS results for specimens after 56 days of immersion at 298 K.

Specimen	R_s (Ω.cm^2)	$R_s + R_{ct}$ (Ω.cm^2)	Z_w (Ω.cm^2)
Uncoated bar	255.95	975.5	1106
Zn coated bar	11897	30173	5.432×10^{15}
Sn coated bar	15129	42163	26632

5. CONCLUSIONS

This research provided strong evidence for the effectiveness of an integrated tin and zinc coating method applied during the simulated temperature of the hot-rolling-process to enhance the resistance of steel rebars against corrosion. The proposed nanometalic coatings improved both structural integrity and surface characteristics, producing compact layers with smaller particle sizes and reduced roughness. The best corrosion protection was achieved in reinforcing bars coated by nano-Sn, which reached an inhibition efficiency of (96.53%) at 298 K after 28 days of immersion in a (3.5%) of sodium chloride solution. Moreover, this sample exhibited the highest solution resistance (15,129 Ω·cm^2) and Warburg impedance (26,632 Ω·cm^2) after 56 days, confirming its strong barrier properties. Samples coated by nano-Zn, also performed effectively, reaching (96.47%) efficiency under the same conditions. Overall, both coatings significantly outperformed the uncoated steel, especially at lower temperatures and shorter exposure times.

References

[1] T. Mohammed, W. Alsaraj, L. A. Zghair, Engineering Technol. & Applied Sci. Res. 14 (2024) 17848. https://doi.org/10.48084/etasr.8729
[2] W. M. Abd El-Gawad, E.A. Mossalam, M. Gharieb, Innov. Infrastruct. Solut 9 (2023) 17. 10.1007/s41062-023-01341-0
[3] D. Kasim, W. Alsaraj, Engineering Technol. & Applied Sci. Res. 15 (2025) 19670. 10.48084/etasr.9218
[4] H. I. Ahmed, AIP Conference Proceedings, 2235 (2020) 020038. https://doi.org/10.1063/5.0008913
[5] A. Goyal, H.S.Pouya, E. Ganjian, P. Claisse, Arabian J. Sci. Eng. 43 (2018) 5035. 10.1007/s13369-018-3303-2
[6] H. Hasan, A. Nooruldeen, H. I. Ahmed, and M. J. Jaafer, Periodicals of Engineering and Natural Sciences (PEN), 8 (2020) 2 727. https://doi.org/10.21533/pen.v8.i2.1100
[7] D. Z. M. Aljaboobi, I. V. Burakova, A. E. Burakov, R. J. Sldozian, A. G. Tkachev, Technical Phys., 69 (2024), 2204 10.1134/S1063784224700579
[8] H. I. Ahmed, AIP Conference Proceedings, 2235 (2020) 020038. https://doi.org/10.1063/5.0008913
[9] A. Jihad, R. J. A. Sldozian, Kadhim, R. F. Kadhim, Eng. Transactions 72 (2024) 22. 10.24423/EngTrans.3206.2025
[10] Y. Zhou, Y. Yu, W. Guo, F. Xing, M. Guo, Cement & Concrete Compos. 152 (2024) 105612. 10.1016/j.cemconcomp.2024.105612
[11] F. A. Cedrim, V. L. S. Almeida, C. A, C. Souza, M. D. Jesus, D. V. Ribeirro, Revista Ibracon Structures & Materials J. 9 (2016) 595. 10.1590/S198341952016000400008

[12] Abraham George, Experimental and Theoretical NANOTECHNOLOGY, 8 (2024) 1 https://doi.org/10.56053/8.1.1
[13] M. Sohail, M. Saleh, N. Al Nuaimi, R. Kahraman, Int. J. l of Building Pathology & Adaptation 37 (2019) 657. 10.1108/IJBPA-12-2018-0088
[14] M. Tadres, Experimental and Theoretical NANOTECHNOLOGY, 8 (2024) 11 https://doi.org/10.56053/8.1.11
[15] https://doi.org/10.1088/2631-8695/ab35f0A. Afshar, S. Jahandari, H. Rasekh, M. Shariati, A. Afshar, A. Shokrgozar, Const. & Building Materials 262 (2020) 120034 10.1016/j.conbuildmat.2020.120044
[16] M. G. Sohail, R. Kahraman, N. Alnuaimi, B. Gencturk, W. Alnahhal, M. Dawood, A. Belarbi, Const. & Building Materials 232 (2020) 117205 10.1016/j.conbuildmat.2019.117206
[17] A. Al-Negheimish, R. Hussain, A. Alhozaimy, D. Singh, Construction and Building Materials 274 (2021) 121921 10.1016/j.conbuildmat.2020.121934
[18] N R. S. Mahmood, et al., Journal of the Mechanical Behavior of Materials, 34 (2025) 1. https://doi.org/10.1515/jmbm-2025-0040
[19] A. Uzunömeroğlu, A. Boğa, S. Pat, İ. Topçu, Arabian J. for Sci. & Eng. 47 (2022) 12789 10.1007/s13369-022-06619-6
[20] C. Das, Z. Haibing, X. Zhao, J. Dai, Const. & Building Materials 394 (2023) 132210 10.1016/j.conbuildmat.2023.132210
[21] J. G. Kim, P. Tan, Experimental and Theoretical NANOTECHNOLOGY, 8 (2024) 17 https://doi.org/10.56053/8.1.17
[22] N. Saniee, H. Elmkhah, M. Molaei, A. Zolriasatein, Int. J. of Eng. 37 (2024) 127 10.5829/IJE.2024.37.01A.35
[23] F. Susetyo, Y. Widiyanto, B. Soegijono, S. Yudanto, S. Ismarwanti, R. Kriswarini, C. Rosyidan, Int. J. Eng. 37 (2024) 1812 10.5829/IJE.2024.37.09C.11
[24] P. Pokorny, N. Prodanovic, K. Hurtig, V. Steinerová, J. Fojt, V. Brožek, Buildings 14 (2024) 1543 10.3390/buildings14061543
[25] Maria S. da Dunla, Experimental and Theoretical NANOTECHNOLOGY, 8 (2024) 23 https://doi.org/10.56053/8.2.23
[26] IQ. S Team, Central Organization for Standardization & Quality Control (COSQC), Portland Cement, Iraq, 1984; No.5 https://www.iso.org/member/308857.html
[27] I. IQ. S Team, Central Organization for Standardization & Quality Control (COSQC), Aggregates from Natural Sources for Concrete and Building Construction, Iraq, 1984; No.45 https://www.iso.org/member/308857.html
[28] Ziyad Khalf Salih, Angham Ayad Kamall-Eldeen, Experimental and Theoretical NANOTECHNOLOGY, 8 (2024) 27 https://doi.org/10.56053/8.2.27
[29] Ghazal Tuhmaz, *Experimental and Theoretical NANOTECHNOLOGY*, *8* (2024) 33 https://doi.org/10.56053/8.2.33
[30] H. A. Abdulaah, A. M. Al- Ghaban, R. A. Anaee. A. Khadom, M. M. Kadhim, J. of Electrochemical Sci. & Eng. 13 (2023) 115 10.5599/jese.1358
[31] Badis Bendjemil, Maram Mechi, Khaoula Safi, Mounir Ferhi, Karima Horchani Naifer, Experimental and Theoretical NANOTECHNOLOGY, 8 (2024) 51 https://doi.org/10.56053/8.3.51
[32] K. Schaefer, A. Miszczyk, Corrosion Sci. 66 (2013) 380 10.1016/j.corsci.2012.10.004
[33] S. A. Naser, R. A. Anaee, H. A. Jaber, Eng. & Technol. J. 41 (2023) 836 10.30684/etj.2023.138741.1404
[34] H. M. Jedy, R. A. Anaee, A. A. Abdulkarim, Eng. & Technol. J. 39 (2021) 565 10.30684/etj.v39i4A.1902
[35] A. M. Ahmed Alwaise, Raqeeb H. Rajab, Adel A. Mahmood, Mohammed A. Alreshedi, Experimental and Theoretical NANOTECHNOLOGY, 8 (2024) 67 https://doi.org/10.56053/8.3.67
[36] X. X. Li, J. Qin, S. Pan, B. Dong, H. Yang, Computational Mate. Sci. 63 (2012) 214 10.1016/j.commatsci.2012.06.029

[37] H. Inui, N. L. Okamoto, S. Yamaguchi, ISIJ Int. 58 (2018) 1550 10.2355/isijinternational.ISIJINT-2018-066
[38] Y. Wang, X. Pandeng, P. Mao, Y. Wang, Z. Zhang, T. He, Z. Fanchao, Y. Yu, F. Yunmiao, J. of Alloys and Compounds 688 (2021) 159139 10.1016/j.jallcom.2021.159139
[39] M. H. Hafiz, R. A. Anaee, R. A. Noor, M. A. Wehib, International J. of Electrochemical Sci. 8 (2013) 12402 10.1016/S1452-3981(23)13276-7
[40] M. Sadeldine, Experimental and Theoretical NANOTECHNOLOGY, 9 (2025) 1 https://doi.org/10.56053/9.1.1
[41] J. Alcántara, D. D. Fuente, B. Chico, J. Simancas, I. Díaz, M. Morcillo, Materials 10 (2017) 406 10.3390/ma10040406
[42] S. A. Naser, R. A. Anaee, H. A. Jaber, A. A. Khadom, Inorganic Chemistry Communications, 165 (2024)112478 10.1016/j.inoche.2024.112478
[43] N. M. Slaber, J. S. Kith, Experimental and Theoretical NANOTECHNOLOGY, 9 (2025) 9 https://doi.org/10.56053/9.1.9
[44] M. Gagné, F. E. Goodwin, M. Leeuwen, Conference: 9th Int. Symp. Steel Bridges 1 (2018) 7 342751453
[45] S. A. Maged, R. A. Anaee, M. T. Mathew, Int. J. of Corrosion and Scale Inhibition 12 (2023) 275 10.17675/2305-6894-2023-12-1-16.
[46] Estabraq Talib Abdullah, Malik Rashid Khasheet, Zainab Naseer Hasheem, Experimental and Theoretical NANOTECHNOLOGY, 9 (2024) 373 https://doi.org/10.56053/9.S.373
[47] H. Li, H. Yu, T. Zhou, B. Yin, S. Yin, Y. Zhang, Materials & Design 84 (2015) 9. https://doi.org/10.1016/j.matdes.2015.06.121
[48] R. A. Anaee, A. A. Abdulkarim, M.T. Mathew, H. M. Jedy, J. of Bio- and Tribo-Corrosion, 7 (2021) 1 10.1007/s40735-020-00440-0

© 2026 The Authors. Published by LPCMA (https://etnano.com). This article is an open access article distributed under the terms and conditions of the Creative Commons Attribution license (http://creativecommons.org/licenses/by/4.0/).